Design and test of the bilateral throwing soil-covering device for straw mulching machine in orchards

Xinhua Zhu[1*], Xiang Gao[1], Xudong Li[1], Shaojie Xu[2]

(1. *College of Mechanical and Electronic Engineering, Northwest A&F University, Yangling 712100, Shaanxi, China*;
2. *Weichai Lovol Heavy Industry Co., Ltd., Weifang 261200, Shandong, China*)

Abstract: Aiming to lack the function of soil covering in the developed orchard straw mulching machine (OSM), a kind of bilateral counter-throwing soil-covering device was developed to eliminate the orchard fire risk caused by the straw layer. The soil-covering device was suspended at the rear of the OSM. Its core component was a pair of throwing wheels installed on both sides of a frame. Hydraulic motors drove the throwing wheels to take soil on-site and cover the straw layer. The adjustment range of the space between the throwing wheels on both sides was 1.4-2.1 m. Based on the analysis of soil-covering quantity, soil-covering width, thickness uniformity of soil layer, and power consumption, the key parameters such as the radius, the number of the vane, and the minimum rotation speed of the throwing wheels were determined. It was proved that the thickness uniformity of the soil layer by bilateral counter-throwing was better than by unilateral, and bottom throwing was better than top throwing. The blade of the soil cutter consisted of a straight blade and a curved blade, and the sliding-cutting angle was 14°-40°. The field test results showed the soil-covering device had good performance with a width of 1.4-2.2 m, a thickness of the soil-covering layer (TSL) of 23.2-40.7 mm, a standard deviation (SD) of 1.4-2.9 mm, width uniformity of 100%, and leakage rate of zero. The established model, between the thickness of soil-covering layer and trenching depth, throwing angle, and rotation speed of the throwing wheels, has a determination coefficient of 0.9757 and can be used to guide the operating parameters. The soil cutter reduced the power consumption and impact load of the throwing wheels by 64.77% and 60.88%, respectively. This work provides a type of new equipment for the mechanization technology of straw mulching in arid and semi-arid orchards.

Keywords: orchard, straw mulching, mechanization, soil-covering device, counter-throwing, uniformity
DOI: 10.25165/j.ijabe.20231601.7010

Citation: Zhu X H, Gao X, Li X D, Xu S J. Design and test of the bilateral throwing soil-covering device for straw mulching machine in orchards. Int J Agric & Biol Eng, 2023; 16(1): 162–171.

1 Introduction

The Loess Plateau is one of the most important apple-producing areas in China, but its problems such as low soil organic matter content, deep soil desiccation, and soil erosion have become the restricting factors for the sustainable development of the fruit industry in this region. Increasing soil carbon content and preserving soil moisture is a critical way to deal with these problems. The total amount of crop straw in China is vast[1, 2], but resource waste and environmental pollution caused by unreasonable utilization of straw are relatively severe[3,4]. Numerous studies have shown that straw mulching is the best way of orchard soil management in arid areas[5-8], with water storage and moisture conservation[9-11], improving soil organic matter content[12-14], suppressing weeds[15,16], reducing soil erosion[17-19] and secondary salinization[20-22], etc., thus improving fruit yield and quality[23,24]. However, the technology has not been widely used due to high labor costs and the orchard fire risk caused by straw. How to reduce costs and eliminate fire hazards is key to the implementation of the technology.

Xu et al.[25] proposed a straw mulching mechanization technology for orchards. This technology needs a special machine to be developed to mulch the crop straw on the ground between tree rows and simultaneously take the soil to cover the straw layer. The role of the soil-covering layer is to eliminate fire risk and prevent the straw layers from piling up by wind or drifting away by rain. The soil-covering layer should be uniform and consistent. Too thick a soil-covering layer is inconducive to straw decomposition and weed control, 20-40 mm is suitable[26]. A self-propelled OSM had been developed, with straw mulching thickness and width adjustable[25]. But the machine does not have the function of soil covering. Therefore, it is necessary to develop a matching soil-covering device for the technology.

There are many existing soil-covering devices, but they are not suitable for the thin soil-covering operation requirements of the OSM. The width of the straw mulch layer between tree rows is generally not less than 1.4 m. The soil-covering device of the grape-burying machine has a large soil-covering amount, large soil-covering thickness, and less uniformity requirement of the soil layer[27]. The film-covering devices for corn planters[28], seedling transplanters[29], and so on are narrow strip-covering devices and are not suitable for the OSM for large-width thin-layer soil covering operation. Therefore, the purpose of this paper is to develop a soil-covering device for the OSM, with good thickness uniformity of soil layer and adjustable soil-covering width, to improve the straw mulching mechanization technology.

Received date: 2021-08-20 **Accepted date:** 2021-11-20
Biographies: Xiang Gao, MS candidate, research interest: design and manufacture of modern agricultural machinery and equipment, Email: 18846428732@163.com; **Xudong Li**, PhD candidate, research interest: agricultural mechanization engineering, Email: lxd0205@nwafu.edu.cn; **Shaojie Xu**, Master, research interest: agricultural machinery equipment and technology, Email: xushaojie1023@163.com.

***Corresponding author: Xinhua Zhu**, PhD supervisor, Professor, research interest: new technology and equipment of agricultural machinery, food processing and rapid testing technology. College of Mechanical and Electronic Engineering, Northwest A&F University, Yangling 712100, Shaanxi, China. Tel: +86-29-87092391, Email: zxh920@nwsuaf.edu.cn.

2 Structure and working principle of the soil-covering device

2.1 Orchard agronomy to soil-covering device design requirements

The row spacing of dwarf close-planting apple orchard is 3.3-4.5 m, the accessible width between the rows is 2.0-2.5 m, the road width for transporting is 6 m[30], the slope of the orchard is no greater than 15°, and the width of a straw mulching layer is 1.4-2.2 m. The soil-covering device should meet the following requirements:

1) The soil-covering device should match with the OSM and can take soil on-site and cover the straw layer with thin soil synchronously. The structure of the soil-covering device should be compact with a retraction width no greater than 1.8 m and the distance between the soil taking point and the tree trunk ≥50 cm.

2) The width of the soil-covering layer is the same as that of the straw mulch layer and adjustable, and the thickness of the soil-covering layer is adjustable from 20 mm to 40 mm with good uniformity and low leakage rate.

2.2 Structure of the soil-covering device

The OSM adopted crawler chassis, with a scraper component equipped at the bottom of the container and a discharge tooth-roller equipped at the rear of the container. Hydraulic motors drive the scraper component and the discharge tooth-roller. The soil-covering device was suspended at the end of the OSM by a four-bar linkage and was lifted by wire rope and hydraulic cylinder (Figure 1a).

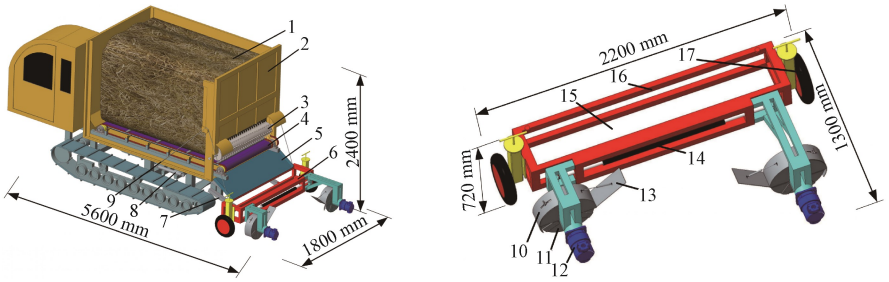

a. Structure diagram of the OSM b. Structure diagram of the soil-covering device

1. Straw 2. OSM 3. Discharge tooth-roller 4. Scraper component 5. Shedding plate 6. Soil-covering device 7. Four-bar linkage 8. Hoist cylinder 9. Wire rope 10. Cover shell 11. Throwing wheels 12. Hydraulic motor 13. Soil-throwing baffle 14. Telescopic hydraulic cylinder 15. Feeding mouth 16. Frame 17. Depth limiting wheel

Figure 1 Structure diagram of the OSM and soil-covering device

The structure of the soil-covering device is shown in Figure 1b. It is mainly composed of frame, soil-throwing mechanism, telescopic hydraulic cylinder, transmission device, and other components. The soil-throwing mechanism primarily consisted of the throwing wheels, the cover shell, and soil-throwing baffle. A pair of throwing wheels were installed on both sides of the frame, and were in staggered throwing trajectory.

The throwing wheels are driven by a hydraulic motor and take and throw the soil in situ, and its structure is shown in Figure 2a. The telescopic mechanism comprised of a telescopic hydraulic cylinder, left and right telescopic frame (Figure 2b), connected with the soil throwing mechanism to adjust the distance between the two throwing wheels. The depth limiting wheels were installed on both sides of the frame to adjust the trenching depth of the throwing wheels. The technical parameters of the OSM and soil-covering device are listed in Table 1.

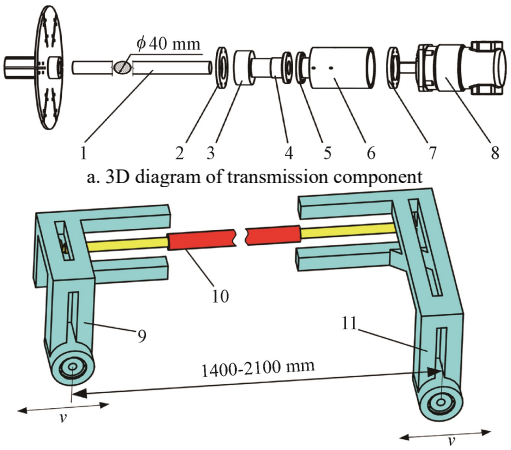

a. 3D diagram of transmission component

b. Diagram of telescopic frame

1. Drive shaft 2. Left end cover 3. Bearing 4. Left half of coupling 5. Right half of coupling 6. Steel sleeve 7. Right end cover 8. Hydraulic motor 9. Left telescopic frame 10. Telescopic hydraulic cylinder 11. Right telescopic frame

Figure 2 Transmission component and telescopic frame structure

Table 1 Main technical parameters of the OSM and soil-covering device

Item	Technical parameters
Power of the OSM/kW	67
The whole vehicle size (length×width×height)/m^3	4.3×2.0×2.4
Load/kg	5000
Soil-covering device (length×width×height)/m^3	1.30×1.80–2.50×0.72
Spacing of the throwing wheels/m	1.4-2.1
Speed/km·h^{-1}	0.5-3.6
Hydraulic system pressure/MPa	16
The width of soil-covering layer/m	1.4-2.2
The thickness of soil-covering layer/mm	23.2-40.7
Rotation speed of the throwing wheels/r·min^{-1}	225-275
Trenching depth of the throwing wheels/cm	8-12

2.3 Working Principle

The working principle of the soil-covering device is shown in Figure 3. When the OSM is working, the scraper component rotates to transport the straw back, and the discharge tooth-roller breaks the straw and spreads it on the ground through the feeding mouth of the soil-covering device. The throwing wheels rotate to take and throw the soil, covering the straw mulch layer evenly. The width of the soil-covering layer, which is slightly larger than the width of the straw mulch layer, can be adjusted by the telescopic hydraulic cylinder and the rotation speed of throwing wheels. The thickness of the soil-covering layer can be adjusted by depth limiting wheels.

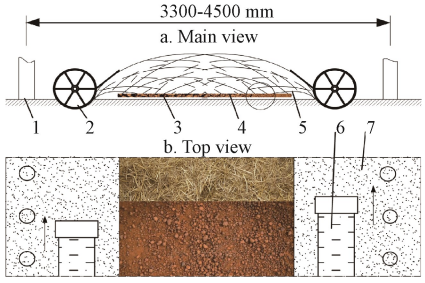

1. Tree trunk 2. Throwing wheel 3. Straw mulch layer 4. Soil-covering layer 5. Soil throwing track 6. Soil trench 7. Ground surface

Figure 3 Scheme diagram of bilateral counter-throwing soil covering

3 Design and analysis of the throwing wheels

3.1 Structure design of the throwing wheels

The throwing wheel consists of the cover shell, the soil cutter, the backplate, the soil-throwing baffle, the vane, etc (Figure 4). The six pieces of vanes are evenly distributed on the backplate of the throwing wheel. The soil cutters were installed on the soil-facing end of each vane to chop the soil and guide it to the vane. The cover shell was mounted on the outer edge of the throwing wheel, concentric with the throwing wheel, and hinged with the soil-throwing baffle to realize the adjustment of the throwing angle and improve soil covering uniformity. The wheel hub was welded on the backplate and was connected to the hydraulic motor. When the soil-covering device is working, the hydraulic motor drives the vanes of the throwing wheels to rotate to cut and throw soil.

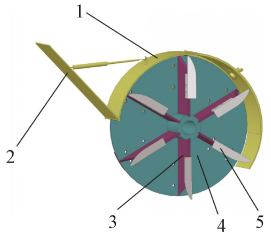

1. Cover shell 2. Soil-throwing baffle 3. Vane 4. Backplate 5. Soil cutter

Figure 4 Structure diagram of the throwing wheel

3.2 Dynamic analysis of soil particles on vanes

The throwing wheel rotates for soil taking and throwing. Assuming that the collisions between the vane of the throwing wheel and the soil particles are inelastic, and the initial velocities of the soil particles sliding outward along the vanes after the collision are zero. The soil was treated as a particles group for simplifying soil motion analysis. In order to obtain the movement rules of soil particles sliding along the vane, the soil particle c on the vane was taken as the research object. The force analysis of soil particle c sliding along the vane is shown in Figure 5. The forces acting on the soil particle c consist of Coriolis force $2m\omega \mathrm{d}l/\mathrm{d}t$, Gravity mg, centrifugal force $mr\omega^2$, normal support force of the vane F_N, and friction force μF_N, along the direction of the vane[31]. Point O, the rotation center of the throwing wheel, was taken as the origin of coordinates. The fixed coordinate axis OZ is vertically downward, while the dynamic coordinate axis OL along the direction of the vane is positive outward and rotates together with the vane. The OZ axis in the vertical direction was taken as the initial position of the vane.

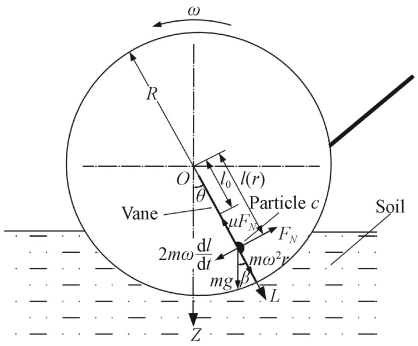

Note: m is the mass of the soil particle, kg; R is the radius of the throwing wheel, mm; l is the dynamic coordinate of the soil particle, mm; l_0 is the initial dynamic coordinate of the soil particle, mm; r is the distance between the soil particle c and point O, mm; ω is the angular velocity of the vane, rad/s; θ is the rotation angle of the vane, (°); β is the angle between Gravity and vane direction, (°), $\beta=\theta$; μ is the friction coefficient of the soil particles along the vane.

Figure 5 Force analysis of the soil particle on the vane surface of the throwing wheel

The differential equation and boundary condition of motion of the soil particle c along the vane are as follows:

$$\begin{cases} m\dfrac{\mathrm{d}^2 l}{\mathrm{d}t^2} = mr\omega^2 + mg\cos\beta - \mu(2m\omega\dfrac{\mathrm{d}l}{\mathrm{d}t} + mg\sin\beta) \\ l\,|_{t=0} = l_0 \\ \dfrac{\mathrm{d}l}{\mathrm{d}t}|_{t=0} = 0 \end{cases} \tag{1}$$

Solving Equation (1) for the dynamic coordinates l of soil particles, then

$$l = C_1 e^{\lambda_1 t} + C_2 e^{\lambda_2 t} + \frac{g(\mu^2-1)}{2\omega^2(\mu^2+1)}\cos\omega t + \frac{g\mu}{\omega^2(\mu^2+1)}\sin\omega t \tag{2}$$

where,

$$\lambda_1 = \omega(-\mu+\sqrt{1+\mu^2}),\ \lambda_2 = \omega(-\mu-\sqrt{1+\mu^2}),$$

$$C_1 = \frac{g}{4\omega^2}[\cos 2\varphi - \sin\varphi] + \frac{1+\sin\varphi}{2}l_0,$$

$$C_2 = \frac{g}{4\omega^2}[\cos 2\varphi + \sin\varphi] + \frac{1-\sin\varphi}{2}l_0,$$

$$\mu = \tan\varphi$$

where, t is the time of the soil particle movement, s; g is the acceleration of gravity, m/s^2; φ is the angle of sliding friction between the soil particles and the vane, (°); n is the rotation speed of the throwing wheel, r/min.

Differentiating Equation (2) with respect to time t, velocities v_r of the soil particles sliding along the vane are:

$$v_r = \frac{\mathrm{d}l}{\mathrm{d}t} = C_1\lambda_1 e^{\lambda_1 t} + C_2\lambda_2 e^{\lambda_2 t} - \frac{g(\mu^2-1)}{2\omega^2(\mu^2+1)}\omega\sin\omega t + \frac{g\mu}{\omega^2(\mu^2+1)}\omega\cos\omega t \tag{3}$$

3.3 Parameters determination of the throwing wheel

3.3.1 Radius determination of the throwing wheel

Assuming that the sum of the trench cross-sectional areas of the two throwing wheels is equal to the cross-sectional area of the soil-covering layer, then

$$S_1 = \frac{1}{2}S_2 k \tag{4}$$

$$S_1 = f(\theta_0)R^2 \tag{5}$$

where, S_1 is the cross-sectional area of the soil trench, m^2; S_2 is the cross-sectional area of soil-covering layer, m^2; k is the effective coefficient of soil used in the throwing process, 0.7; θ_0 is the angle between the axis of the throwing wheel and the connection of both sides of the soil trench, (°); $f(\theta_0)$ is a function of θ_0, which is $\frac{2\theta_0}{360}\pi - \sin\theta_0\cos\theta_0$.

According to the requirements of soil covering operation, the maximal width of soil covering was taken as 2.2 m, and the thickness was taken as 0.03 m. Assuming that the trenching depth is half of the radius of the throwing wheel, then the radius of the throwing wheel was calculated as 0.194 m, taken as R=0.2 m.

3.3.2 Determination of the number of the vane

The number of vanes of the throwing wheel will affect the resistance and the soil covering uniformity. The soil cutting resistance of vanes is positively correlated with soil cutting thickness δ, and the total soil cutting length d_{sum}. If there is only one vane in the soil trench to cut soil, the soil cutting resistance fluctuates greatly, which is not conducive to operation stability. Therefore, at least two vanes are needed to cut soil at the same time. The soil cutting lengths of Vane a and Vane b in the soil trench were analyzed (Figure 6).

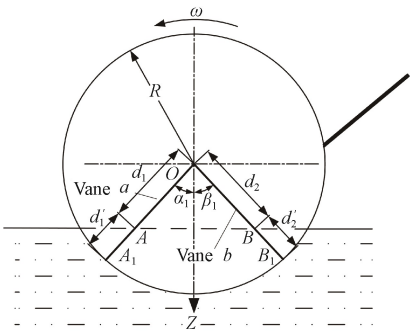

Note: α_1 is the angle between Vane *a* and *OZ* axis, (°); β_1 is the angle between Vane *b* and *OZ* axis, (°); *A* is the intersection point between Vane *a* and ground surface; A_1 is the intersection point between Vane *a* and soil trench circular edge; *B* is the intersection point between Vane *b* and ground surface; B_1 is the intersection point between Vane *b* and soil trench circular edge; d_1 is the length of the unburied segment of Vane *a*, mm; d_1' is the length of soil cutting of Vane *a*, mm; d_2 is the length of the unburied segment of Vane *b*, mm; d_2' is the length of soil cutting of Vane *b*, mm.

Figure 6 Analysis of soil cutting length of vanes

It can be seen from Figure 6 that the calculation formula of soil cutting length of the vane is as follows:

$$\begin{cases} d_1' + d_2' = 2R - d_1 - d_2 \\ d_1 = \dfrac{R}{2 \cdot \cos\alpha_1} \\ d_2 = \dfrac{R}{2 \cdot \cos\beta_1} \\ \alpha_1 + \beta_1 = \dfrac{2\pi}{N} \end{cases} \tag{6}$$

The soil cutting thickness δ of a single vane is

$$\delta = \frac{60 \cdot v \cdot 1000}{n \cdot N} \tag{7}$$

where, δ is the soil cutting thickness of a single vane, mm; v is the speed of the OSM, m/s; N is the number of the vane; n is the rotation of the throwing wheel. Taking d_{sum} as the total soil cutting length, mm. Then, $\delta \times d_{sum}$ of the vanes was obtained as follows:

$$\delta \cdot d_{sum} = (d_1' + d_2') \cdot \delta \tag{8}$$

The mean $\delta \times d_{sum}$ was shown in Figure 7.

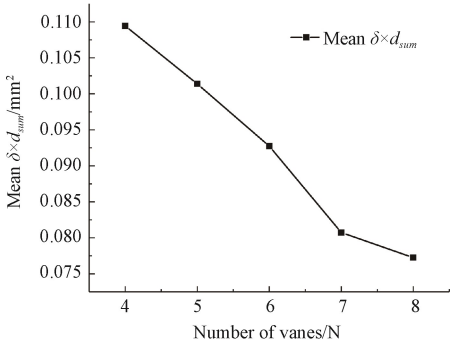

Figure 7 Digram of mean $\delta \cdot d_{sum}$ changes with vane number

According to Equations (6)-(8) and Figure 7, the mean resistance (mean $\delta \cdot d_{sum}$) of soil cutting decreases with the rise of the number of vanes. When the number of vanes is more than six, with the increase of vane number and reduction of the cutting soil amount of single vane, l_0 will increase (Figure 5), and the movement time of the soil along the vane will reduce. Thus, the variation range of ejection velocity will decrease, which results in a concentration of the drop points of soil particles and poor uniformity of the soil-covering layer. Therefore, the number of vanes was determined as six.

3.4 Analysis of unilateral throwing and bilateral counter throwing

There are two kinds of throwing methods for the soil-covering device[32], unilateral throwing and bilateral counter throwing (Figure 3). It is necessary to determine which one performs well by discrete element mothed (DEM) simulation.

3.4.1 Construction of simulation model of soil covering

EDEM 2018 (DEM Solutions Ltd, UK) was used to simulate the soil throwing process of the throwing wheel. The soil contact model was set as Hertz-Mindlin with Bonding. The material parameters of the soil and the contact parameters between the soil particles were quoted from the literature[33]. The dimensions of the soil trench and the carrier plate were 500 mm×2000 mm×145 mm and 2500 mm×2000 mm, respectively (Figure 8). The diameter of the throwing wheel was 400 mm. The operating parameters in the simulation process were: the rotation speed of the throwing wheel was 250 r/min; the trenching depth was 100 mm; the throwing angle was 40°; the forward speed was 0.278 m/s.

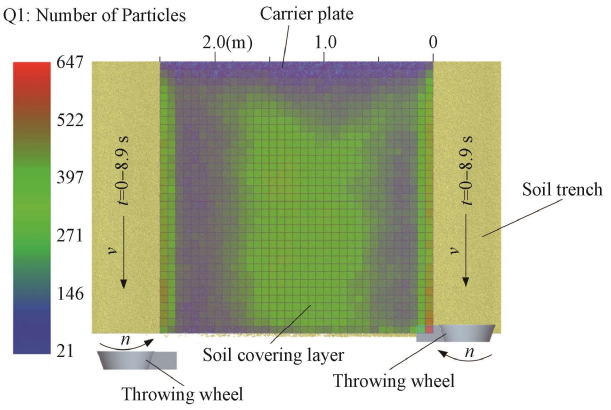

a. Bilateral counter throwing

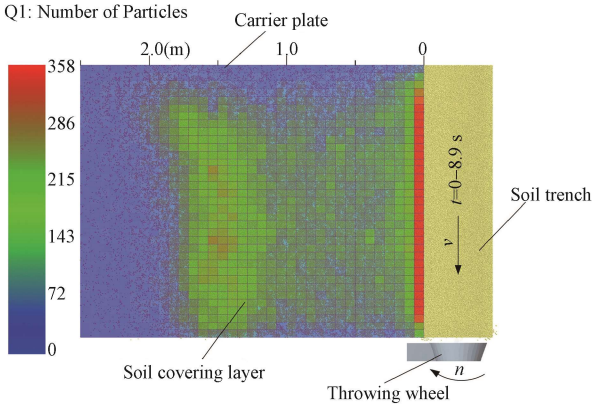

b. Unilateral throwing

Figure 8 Simulation comparison between the unilateral and bilateral throwing

3.4.2 Analysis of simulation results of unilateral throwing and bilateral counter throwing

In the simulation model of bilateral counter throwing, the two throwing wheels were located on both sides of the carrier plate and were staggered in the direction of front and back (Figure 8a). In the simulation model of unilateral throwing, the throwing wheel was located on one side of the carrier plate (Figure 8b). According to the color bar, the soil particles for unilateral throwing

were less and gathered in the distal end. In contrast, the soil particle number for bilateral counter throwing was larger and uniformly distributed in the soil covering area, indicating that bilateral counter throwing was better than unilateral throwing, consistent with the theoretical analysis.

3.5 Analysis of top throwing and bottom throwing

The bottom throwing and top throwing are shown in Figure 9. The uniformity and dynamic power consumption of soil throwing need to be analyzed to select the soil throwing type.

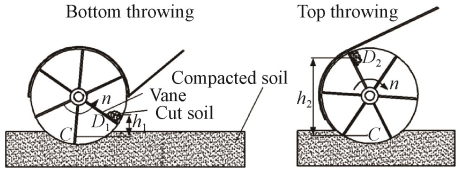

Note: h_1 is the lifting height of soil by bottom throwing, m; h_2 is the lifting height of soil by top throwing, m; C is the location of the soil mass center for each cut; D_1 is the position of the mass center by bottom throwing; D_2 is the position of the mass center by top throwing.

Figure 9 Analysis of top throwing and bottom throwing

3.5.1 Uniformity of soil-covering layer

As the throwing wheel rotates to collect soil, the collected soil particles are accelerated along the vanes and rotate with the wheel, and are thrown out when they reach the end of the vanes. When bottom throwing, the velocity decomposition of the soil particle moving to the end of the vane is shown in Figure 10.

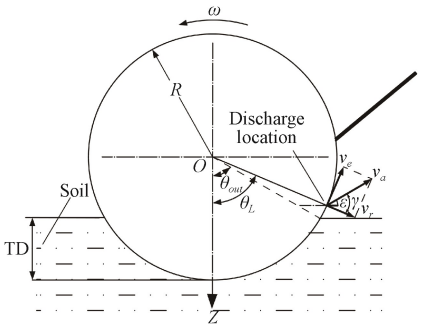

Note: θ_{out} is the rotation angle of the vane when it is rotating out the soil trench, (°); θ_L is the rotation angle of the vane when soil particles reach the end of the vane, (°); v_e is the rotation speed of soil particles when reaching the end of the vane, m/s; v_a is the ejection velocity of soil particles at the end of the vane, which is the resultant velocity of v_r and v_e, m/s; ε is the ejection-angle, (°); TD is the soil trenching depth of vanes, mm. v_r is the speed of soil particles sliding outward along the vane when reaching the end of the vane, m/s; γ is the angle between v_r and v_a, (°);

Figure 10 Analysis of the soil particle movement on the vane of the throwing wheel

When the soil particle moves to the end of the vane, the calculation formula of vane rotation angle θ_L is

$$\theta_L = \frac{2\pi n \cdot t_1}{60} \tag{9}$$

where, t_1 is the time for soil particles to move from the initial position on the vane to the end of the vane.

When $t=t_1$, the soil particle moves to the end of the vane, and its coordinate $l=R$. According to Equations (2), (3), and (9), the vane rotation angle θ_L and the velocity v_r of the soil particle sliding along the vane when the soil particle moves to the end of the vane at different initial displacements l_0 can be obtained.

The ejection velocity v_a and rotation speed v_e of soil particles at the end of the vane is

$$v_a = \sqrt{v_e^2 + v_r^2} \tag{10}$$

$$v_e = \omega \cdot R \tag{11}$$

When the soil particle reaches the end of the vane, the angle γ between v_r and v_e is obtained as,

$$\gamma = \arctan(\frac{v_e}{v_r}) \tag{12}$$

The rotation angle θ_{out} of the vane from the initial position to the position when it leaves the soil trench is

$$\theta_{out} = \arccos(\frac{R - TD}{R}) \cdot \frac{180}{\pi} \tag{13}$$

Combining Equations (12) and (13), the angle ε between ejection velocity v_a and horizontal direction is as follows:

$$\varepsilon = [\gamma - (\frac{\pi}{2} - \theta_L)] \cdot \frac{180}{\pi} \tag{14}$$

Assuming that the initial position of the vane is where when the angle between the vane and the OZ axis is zero. The rotation speed n of the throwing wheel, the soil trenching depth (TD), and the friction angle φ between soil particles and vanes are 250 r/min, 0.1 m, and 30°, respectively. When using bottom throwing, the movement data of soil particles are listed in Table 2:

Table 2 Data of soil particles movement when bottom throwing

Initial dynamic coordinate l_0/m	Rotation angle θ_L/(°)	Projectile–angle ε/(°)	Ejection velocity v_a /m·s^{-1}
0.080	97.357	63.885	6.277
0.100	78.617	45.267	6.268
0.124	60.106	27.658	6.205
0.125	59.396	60.000	5.236

1) Bottom throwing: as listed in Table 2, shown in Figures 5, 9, and 10. Suppose the initial dynamic coordinate l_0 of the soil particles is less than 0.124 m. In that case, the ejection velocity v_a and projectile angle ε change according to the initial dynamic coordinate l_0, the range of them is 6.205-6.277 m/s and 27.658°-63.885°, respectively. It means the soil particles fall far and disperse. On the other hand, suppose the initial dynamic coordinate l_0 of the soil particles is in the range of 0.125-0.200 m, the soil particles are ejected from the end of the vane with the same ejection velocity v_a and the same projectile angle ε, and the falling points are close and relatively concentrated. Generally speaking, the drop points of soil particles under the condition of bottom throwing are relatively dispersed, and the thickness uniformity is good.

2) Top throwing: under this condition, the ejection point is at the top of the throwing wheel. The vane with soil particles has to travel around the circle for a long time to reach the top, all soil particles have moved to the end of the vane and collided with the constraint body (shell), and the velocity v_r decreases to zero. When passing the projectile point, the ejection velocity v_a and projectile angle ε of all the soil particles are the same respectively, so the landing points of the soil particles are concentrated by top throwing with a worse thickness uniformity.

3.5.2 Analysis of simulation results of top and bottom throwing

The simulation results of top throwing and bottom throwing are shown in Figure 11. The simulation parameters are the same as Section 3.4.2. For top throwing, the soil particles are distributed centrally at the far end of the carrier plate (Figure 11). In contrast, for bottom throwing, the soil particles are distributed relatively uniformly along the width of the carrier plate. It shows that the uniformity of bottom throwing is better than top throwing, consistent with the theoretical analysis results.

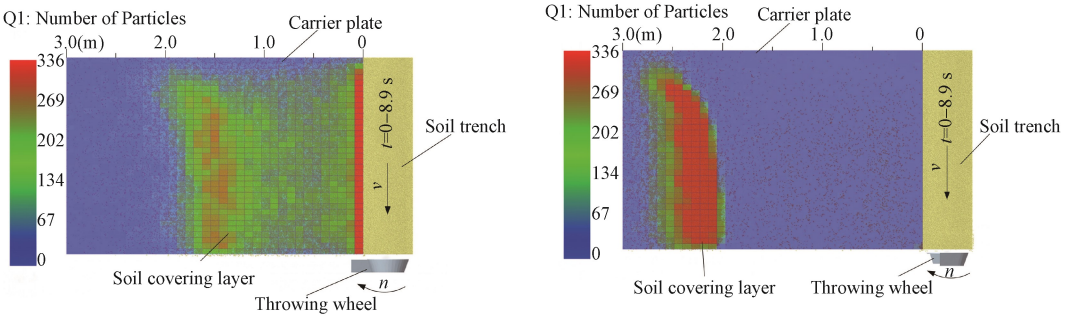

a. Bottom throwing b. Top throwing

Figure 11 Simulation results of top and bottom throwing

3.5.3 Analysis of dynamic power consumption of soil throwing

The power consumption analysis of bottom throwing and top throwing of the throwing wheel is shown in Figure 9:

The energy consumed by the throwing wheel is that the vanes impact the soil particles in the process of rotation, driving the soil particles until they are thrown out, and the soil particles have a certain kinetic energy. According to the functional relationship, the power consumed by bottom throwing and top throwing of the throwing wheel is shown as follows respectively:

$$W_1 = m_1 g h_1 + \frac{1}{2} m v_{a1}^2 + W_{f1} \tag{15}$$

$$W_2 = m_1 g h_2 + \frac{1}{2} m v_{a2}^2 + W_{f2} \tag{16}$$

where, m_1 is the mass of the soil particles thrown by the vane once, kg; W_1 is the power consumed of the throwing wheel by top throwing, J; W_2 is the power consumed of the throwing wheel by bottom throwing, J; v_{a1} is the velocity of soil mass center when it leaves the vane by top throwing, m/s; v_{a2} is the velocity of soil mass center when it leaves the vane by bottom throwing, m/s; W_{f1} is the power consumed by the friction and collision between soil, cover shell, and vane by top throwing, J; W_{f2} is the power consumed by the friction and collision between soil, cover shell, and vane by bottom throwing, J.

Further analysis shows, $v_{a1}=v_{a2}$, $mgh_1>mgh_2$, and $W_{f1}>W_{f2}$. So, the power consumed by the throwing wheel by top throwing is higher than that by bottom throwing.

By comparing the uniformity and power consumption of the throwing wheel by top and bottom throwing, the uniformity of soil covering by bottom throwing is better than that by top throwing, and the power consumption by bottom throwing is less than that by top throwing. Meanwhile, by top throwing, the soil contact with the shell, and the throwing wheel is easily stuck by gravel in orchard operation. Therefore, bottom throwing was selected as the throwing type for the soil-covering device.

3.6 Determination of the minimum rotation speed of the throwing wheel

In order to meet the requirement of soil-covering width, the maximum displacement of soil particles should be more than the soil-covering width X. Therefore, the minimum speed $n_{\min}$ of the vane of the throwing wheel is

$$n_{\min} \geq \sqrt{\frac{X \cdot g}{R^2 \sin 2\varepsilon}} \cdot \frac{60}{2\pi} \tag{17}$$

where, $n_{\min}$ is the minimum rotation speed of the throwing wheel, r/min; X is the soil-covering width which is 2.2 m.

By calculation, the lowest rotation speed $n_{\min}$ of the throwing wheel should be no less than 220.02 r/min. Therefore, the minimum speed of the throwing wheel was taken as 220 r/min.

3.7 Design of the soil cutter

The soil cutter is a crucial component to reduce the soil taking resistance of the throwing wheel and improve the stability of soil throwing. Comprehensively considering the soil cutter's soil cutting and guiding performance, the blade was designed as a straight cutting edge and curve blade section. The curve blade section was designed as an eccentric arc curved blade. The sliding-cutting angle of the soil cutter is shown in Figure 12a.

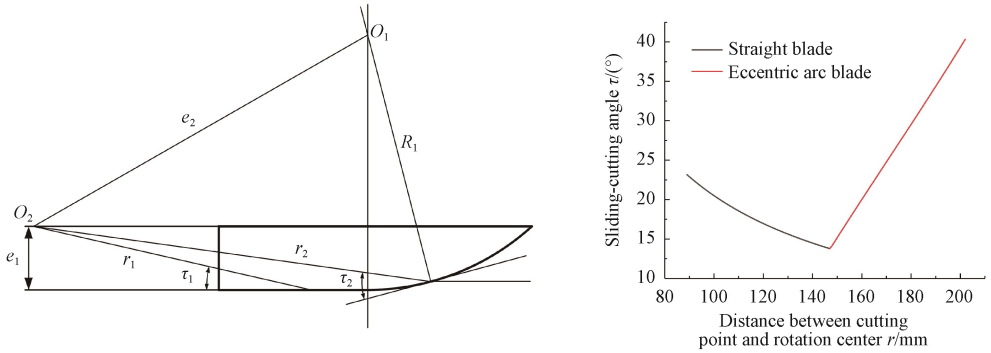

Note: O_1 is the center of the curved blade; O_2 is the rotation center of the soil cutter; e_1 is the distance between the straight cutting edge and the rotation center O_2, mm; e_2 is the distance between the curved blade center O_1 and the rotation center O_2, mm; r_1 is the radius of rotation at the cutting point of the straight cutting edge, mm; r_2 is the radius of rotation at the cutting point of the curved blade, mm; R_1 is the radius of the curved blade, mm; τ_1 is the sliding-cutting angle of the straight cutting edge, (°); τ_2 is the sliding-cutting angle of the curved blade, (°).

a. Sliding-cutting angle diagram of soil cutter b. Sliding-cutting angle at different points of the blade

Figure 12 Sliding-cutting angle of soil cutter

The formulas of the sliding-cutting angle of the straight cutting edge and the eccentric arc curved blade are as follows[34], respectively.

$$\tau_1 = \arcsin(e_1 / r_1) \tag{18}$$

$$\tau_2 = \arcsin[(R_1^2 + r_2^2 - e_2^2) / 2R_1 r_2] \tag{19}$$

According to Equations (18) and (19), the sliding-cutting angle of each point of the eccentric arc curved blade is different. The sliding-cutting angle τ_1 of the straight cutting edge gradually decreases from left to right, and the sliding-cutting angle τ_2 of the eccentric arc curved blade gradually increases from left to right. During soil cutters installation, the eccentricity of the straight cutting edge can be appropriately increased, thus increasing the value of the sliding-cutting angle. The sliding-cutting angle of the soil cutters was designed as 14°-40° (Figure 12b). The design ensured the sliding-cutting angle greater than the friction angle of most types of soil.

According to the trenching depth and the minimum sliding-cutting angle, the critical parameters of the soil cutter were calculated (Figure 13a). The 3D model is shown in Figure 13b.

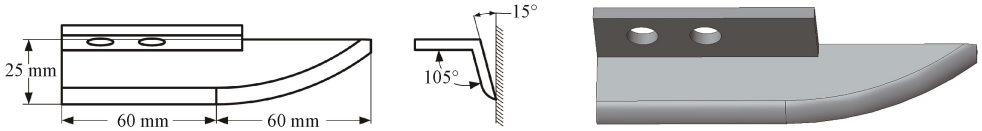

a. Structure diagram of soil cutter b. 3D diagram of soil cutter

Figure 13 Structure diagram of soil cutter

4 Experiment on soil covering

4.1 Experimental methods

The experiment was carried out in March 2019 at the experiment field of Northwest A&F University, Yangling, China. The soil compactness was 5680 kPa, the wet basis moisture content was 12.13%, and the bulk density was 1237 kg/m^3. A plastic-laying device was installed on the soil-covering device to measure the thickness of the soil-covering layer accurately. The soil-covering layer was separated from the subsoil by plastic film. In the preliminary test, the soil-covering width was adjustable from 1.4 to 2.2 m, the width uniformity was 100%, and the leakage rate was zero. Therefore, the soil-covering width, width standard deviation, and leakage rate were no longer considered in the formal test.

4.1.1 Orthogonal experimental design

The main factors affecting the uniformity of soil covering were determined as the speed of the throwing wheel, trenching depth, and throwing angle based on the motion analysis and bench-test[32] of soil covering. A three-factor/three-level orthogonal test was designed. The rotation speed of the throwing wheel X_1, trenching depth X_2, and throwing angle X_3 were taken as experimental factors. The thickness of soil-covering layer (TSL) and its standard deviation (SD) were taken as experimental indexes, representing thickness accuracy and thickness uniformity, respectively. According to the bench-test, the operating parameters were as follows: the rotation speed of the throwing wheel was 225-275 r/min, the soil trenching depth was 8-12 cm, and the throwing angle was 35°-45°. Experiment was repeated twice and the average value was taken as the result. The test scheme is listed in Table 3. The software of Design-expert 10.0 (Statease, MN, USA) was used to analyze the variance of the regression equation of the orthogonal test, and the results are listed in Table 4.

Table 3 Soil covering test of the soil-covering device

No.	Factors			Thickness of soil covering layer (TSL)/mm	Standard Deviation (SD)/mm
	Rotation speed X_1/r·min^{-1}	Trenching depth X_2/cm	Throwing angle X_3/(°)		
1	275	12	40	35.8	2.4
2	250	8	45	26.1	2.0
3	225	8	40	27.1	1.9
4	250	10	40	37.9	1.5
5	275	10	45	27.9	1.4
6	250	12	35	38.5	2.9
7	250	8	35	26.5	1.5
8	275	10	35	33.3	2.1
9	250	10	40	35.6	1.9
10	250	12	45	37.0	2.9
11	225	10	35	38.6	2.4
12	225	12	40	40.7	2.6
13	250	10	40	36.7	1.5
14	225	10	45	36.7	1.8
15	250	10	40	36.9	1.6
16	250	10	40	36.4	1.6
17	275	8	40	23.2	1.4

Table 4 Variance analysis of regression model

Source	TSL				SD			
	Sum of squares	DF	F value	p-value	Sum of squares	DF	F value	p-value
model	453.81	9	31.24	<0.0001	3.58	9	4.99	0.0228
X_1	65.55	1	40.62	0.0004	0.24	1	3.07	0.1230
X_2	301.35	1	186.72	<0.0001	2.00	1	25.09	0.0015
X_3	10.58	1	6.56	0.0375	0.08	1	1.00	0.3498
X_1X_2	0.25	1	0.15	0.7056	0.022	1	0.28	0.6117
X_1X_3	3.06	1	1.90	0.2108	0.0025	1	0.031	0.8645
X_2X_3	0.30	1	0.19	0.6781	0.063	1	0.78	0.4053
X_1^2	8.85	1	5.49	0.0517	0.003184	1	0.040	0.8473
X_2^2	53.06	1	32.88	0.0007	0.77	1	9.65	0.0172
X_3^2	5.33	1	3.30	0.1120	0.32	1	4.07	0.0835
Residual error	11.30	7			0.56	7		
Lack of fit	8.52	3	4.09	0.1037	0.45	3	5.56	0.0655
Pure error	2.78	4			0.11	4		
Total	465.10	16			4.14	16		

4.1.2 Resistance test of soil cutter

In the soil covering test, the resistance reduction test of the soil cutter in the soil-covering device was carried out simultaneously. The handheld hydraulic tester (CHPM-480: Shenzhen Renault

Intelligent Technology Co., Ltd.) was connected to measure the flow and pressure of the hydraulic circuit of the driving motor in the throwing wheel. Then the power consumption of the throwing wheel was calculated. The operating parameters were as follows: the rotation speed of the throwing wheel was 250 r/min, the soil trenching depth was 10 cm, and the throwing angle was 40°. The test process is shown in Figure 14. Origin2017 (OriginLab Co., Northampton, USA) was applied to process and analyze the data.

a. Soil covering test process b. Effect of soil covering test

Figure 14 Test of soil covering

4.2 Results and analysis

4.2.1 Test results

The results of the soil covering test are shown in Figure 14 and Table 3. The results showed that the uniformity of the soil covering was excellent, with a flexible width of the soil covering of 1.4-2.2 m and an adjustable thickness of the soil-covering layer of 23.2-40.7 mm. The soil cutter significantly reduced the soil taking resistance of the soil-covering device.

4.2.2 Regression models of TSL, SD, and variance analysis

The quadratic polynomial response surface regression models of TSL and SD concerning the factors were established, respectively, as shown in Equations (20) and (21).

$$\begin{aligned} TSL = &-355.4125 + 1.3755X_1 + 23.16875X_2 + 5.395X_3 \\ &- 0.005X_1X_2 - 0.007X_1X_3 - 0.0275X_2X_3 \\ &- 0.00232X_1^2 - 0.8875X_2^2 - 0.045X_3^2 \end{aligned} \quad (20)$$

$$\begin{aligned} SD = &29.6175 - 0.036X_1 - 1.7625X_2 - 0.733X_3 \\ &+ 0.0015X_1X_2 - 0.0002X_1X_3 - 0.0125X_2X_3 \\ &+ 0.000044X_1^2 + 0.10687X_2^2 + 0.0111X_3^2 \end{aligned} \quad (21)$$

According to the variance analysis in Table 4, the p-value of the TSL model was <0.0001, indicating the TSL model was highly significant. The p-value of the SD model was 0.0228, telling the SD model was significant. The p-value of lack of fit for the two models was more than 0.05 (0.1037 and 0.0655, respectively). The determination coefficient R^2 was 0.9757 for TSL and 0.8652 for SD, respectively, indicating that regression models fit well and could guide the adjustment of operating parameters of the prototype.

The factor order for the TSL model was X_2, X_1, and X_3 according to the regression coefficient. The factor order for the SD model was X_2, X_1, and X_3 according to the regression coefficient.

4.2.3 Verification of the TSL model

In order to verify the accuracy of the thickness model of the soil-covering device, five groups of parameter combinations of the rotation speed, trenching depth, and throwing angle were randomly set and the corresponding soil-covering thickness was measured. The results showed that the value of SD was 1.8-3.5 mm and the value of Root Mean Squared Error was 0.432. The measured data of soil-covering thickness were compared with the calculated value based on soil-covering thickness model, the results are shown in Figure 15. The determination coefficient between the calculated value and measured value of soil-covering thickness model was 0.9569, which indicated that the soil-covering thickness model fitted well. The model can be used to guide the adjustment of operation parameters in the operation.

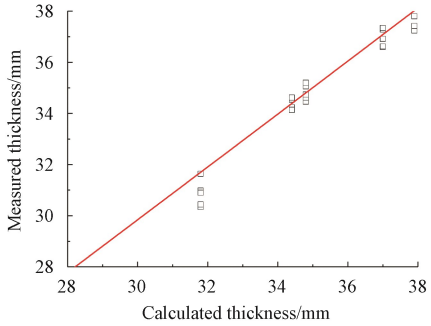

Figure 15 Relationship between measured value and calculated value of thickness model of soil-covering device

4.2.4 Power consumption reduction of soil cutter

Under the given working parameters in 4.1.2, the mean power consumption and peak power consumption with and without the soil cutter were obtained (Figure 16), respectively.

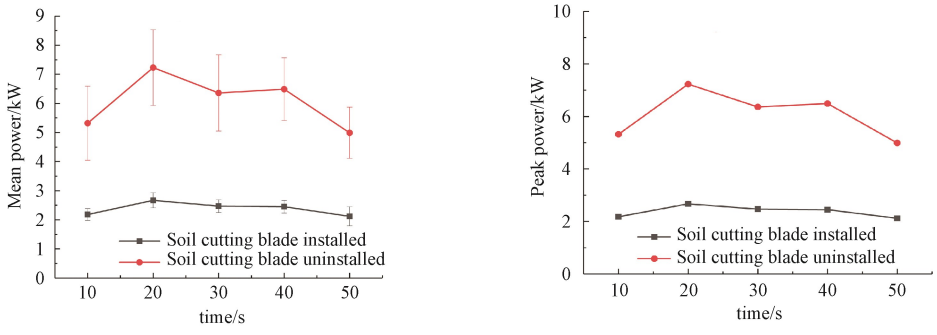

a. Mean power b. Peak power

Figure 16 Comparison of power consumption with and without the soil cutter

The comparison showed that the soil cutter significantly decreased the throwing wheel's power consumption and the impact load by 64.77% and 60.88%, respectively, improving the performance and operation stability of the soil-covering device.

4.2.5 Experiment in orchard

The experiment of mechanized straw mulching was carried out in an apple orchard of the Futus Company in Yangling, China. The row spacing of the orchard was 3.5 m, and the plant spacing was 1.2 m. The operating parameters of the soil-covering device were consistent with the resistance test of soil cutter in Section4.1.2. The test is shown in Figure 17, the thickness of soil covering-layer (TSL) was 25.3-38.5 mm, which met the design requirements.

a. Test of straw mulching and soil covering b. Operation effect

Figure 17 Field test in apple orchard

5 Conclusions

Aiming to lack the function of soil covering in the developed OSM, a bilateral counter-throwing soil-covering device was developed. Through theoretical analysis and field tests, the style of soil throwing and the appropriate operating parameters of the soil-covering device were determined. The main conclusions are as follows:

1) Bilateral counter-throwing soil-covering device was developed for OSM. The device was composed of a frame, soil throwing component, telescopic hydraulic cylinder, transmission device, and other components. Driven by a hydraulic motor, the paired throwing wheels are able to take soil on site. The adjustment range of the spacing between the throwing wheels on both sides is 1.4 -2.1 m.

2) By analyzing the amount of soil taken and the amount of soil covered, the vane radius of the throwing wheel was determined to be 0.2 m. The number of the vanes was determined as six. Bilateral throwing was better than unilateral throwing, and bottom throwing is better than top throwing. According to the width of the soil covering, the minimum rotation speed of the throwing wheel was determined as 220 r/min.

3) The blade of the soil cutter was designed with a straight blade section and a curved blade section. The sliding-cutting angle of the soil cutter was designed to be 14°-40°, which is greater than the friction angle of most types of soil.

4) The field test results show that the soil-covering width is adjustable from 1.4 m to 2.2 m, the width uniformity was 100%, and the rate of leakage cover was zero; The soil-covering thickness was adjustable from 23.2 mm to 40.7 mm. The TSL regression model with respect to the rotation speed, trenching depth, and throwing angle was established with a determination coefficient of 0.9757, which indicates the model could be used to guide the adjustment of operation parameters. The power consumption and impact load of the throwing wheel were reduced by 64.77% and 60.88%, respectively. Thus, the performance of the soil-covering device was significantly improved by the designed soil cutter. The soil-covering device cooperating with the orchard straw mulching machine realized the mechanized straw mulching in the arid and semi-arid orchards.

Acknowledgements

The authors acknowledge the financial support provided by the Science and Technology Major Project of Shaanxi Agricultural Synergy Innovation and Extension Alliance (Grant No. LMZD201703) and Shaanxi Province Key R&D Program Project (Grant No. 2022NY-204, 2023-ZDLSF-62).

[References]

[1] Wang X Y, Yang L, Steinberger Y, Liu Z X, Liao S H, Xie G H. Field crop residue estimate and availability for biofuel production in China. Renewable & Sustainable Energy Reviews, 2013; 27: 864–875.

[2] Wang Y J, Bi Y Y, Gao C Y. The assessment and utilization of straw resources in China. Agricultural Sciences in China, 2010; 9(12): 1807–1815.

[3] Li H, Dai M W, Dai S L, Dong X J. Current status and environment impact of direct straw return in China's cropland - A review. Ecotoxicology and Environmental Safety, 2018; 159: 293–300.

[4] Prasad R, Shivay Y S. Management options to alleviate the menace of rice (*Oryza sativa*) straw burning - An overview. Indian Journal of Agricultural Sciences, 2018; 88(11): 3–12.

[5] Andersen L, Kuhn B F, Bertelsen M, Bruus M, Larsen S E, Strandberg M. Alternatives to herbicides in an apple orchard, effects on yield, earthworms and plant diversity. Agriculture Ecosystems & Environment, 2013; 172: 1–5.

[6] Garcia-Orenes F, Cerda A, Mataix-Solera J, Guerrero C, Bodi M B, Arcenegui V, et al. Effects of agricultural management on surface soil properties and soil-water losses in eastern Spain. Soil & Tillage Research, 2009; 106(1): 117–123.

[7] Mandal A, Majumder A, Dhaliwal S S, Toor A S, Mani P K, Naresh R K, et al. Impact of agricultural management practices on soil carbon sequestration and its monitoring through simulation models and remote sensing techniques: A review. Critical Reviews in Environmental Science and Technology, 2020; 49p. doi: 10.1080/10643389.2020.1811590.

[8] Xu X R, Pei J B, Xu Y D, Wang J K. Soil organic carbon depletion in global Mollisols regions and restoration by management practices: A review. Journal of Soils and Sediments, 2020; 20(3): 1173–1181.

[9] Fang K K, Li H K, Wang Z K, Du Y F, Wang J. Comparative analysis on spatial variability of soil moisture under different land use types in orchard. Scientia Horticulturae, 2016; 207: 65–72.

[10] Wang H, Wang C B, Zhao X M, Wang F L. Mulching increases water-use efficiency of peach production on the rainfed semiarid Loess Plateau of China. Agricultural Water Management, 2015; 154: 20–28.

[11] Mahdavi S M, Neyshabouri M R, Fujimaki H, Heris A M. Coupled heat and moisture transfer and evaporation in mulched soils. Catena, 2017; 151: 34–48. doi:10.1016/j.catena.2016.12.010.

[12] Wang Y J, Liu L, Luo Y, Awasthi M K, Yang J F, Duan Y M, et al. Mulching practices alter the bacterial-fungal community and network in favor of soil quality in a semiarid orchard system. Science of the Total Environment, 2020; 725: 1–13.

[13] Zhang R Q, Huang Q Q, Yan T Y, Yang J F, Zheng Y, Li H K, et al. Effects of intercropping mulch on the content and composition of soil

dissolved organic matter in apple orchard on the loess plateau. Journal of Environmental Management, 2019; 250: 1–9.

[14] Zhao S C, Li K J, Zhou W, Qiu S J, Huang S W, He P. Changes in soil microbial community, enzyme activities and organic matter fractions under long-term straw return in north-central China. Agriculture Ecosystems & Environment, 2016; 216: 82–88.

[15] Hammermeister A M. Organic weed management in perennial fruits. Scientia Horticulturae, 2016; 208: 28–42.

[16] Hussain S, Sharma M K, War A R, Hussain B. Weed management in apple cv. royal delicious by using different orchard floor management practices. International Journal of Fruit Science, 2020; 20(4): 891–921.

[17] Keesstra S D, Rodrigo-Comino J, Novara A, Gimenez-Morera A, Pulido M, Di Prima S, et al. Straw mulch as a sustainable solution to decrease runoff and erosion in glyphosate-treated clementine plantations in Eastern Spain. An assessment using rainfall simulation experiments. Catena, 2019; 174: 95–103.

[18] Li R, Li Q G, Pan L D. Review of organic mulching effects on soil and water loss. Archives of Agronomy and Soil Science, 2021; 67(1): 136–151.

[19] Prosdocimi M, Tarolli P, Cerda A. Mulching practices for reducing soil water erosion: A review. Earth-Science Reviews, 2016; 161: 191–203.

[20] Dong S, Wan S, Kang Y, Sun J. Effects of different mulching methods on water and salt distribution in soil and the growth of Lycium barbarum L. in saline land under drip irrigation. Chinese Journal of Applied and Environmental Biology, 2018; 24(1): 53–59.

[21] Li Y Y, Pang H C, Han X F, Yan S W, Zhao Y G, Wang J, et al. Buried straw layer and plastic mulching increase microflora diversity in salinized soil. Journal of Integrative Agriculture, 2016; 15(7): 1602–1611.

[22] Zhao Y G, Li Y Y, Wang J, Pang H C, Li Y. Buried straw layer plus plastic mulching reduces soil salinity and increases sunflower yield in saline soils. Soil & Tillage Research, 2016; 155: 363–370.

[23] Chen Y X, Wen X X, Sun Y L, Zhang J H, Wu W, Liao Y C. Mulching practices altered soil bacterial community structure and improved orchard productivity and apple quality after five growing seasons. Scientia Horticulturae, 2014; 172: 248–257.

[24] Liang X M, Chen Q, Rana M S, Dong Z H, Liu X D, Hu C X ,et al. Effects of soil amendments on soil fertility and fruit yield through alterations in soil carbon fractions. Journal of Soils and Sediments, 2021; 21(7): 2628–2638.

[25] Xu S J, Zhu X H, Wang D Y. Design and experiment on straw mulching machine in arid orchards. Journal of China Agricultural University, 2019; 24(7): 122–130. (in Chinese)

[26] Wang Qingjiang. Study on straw mulching model and straw Mechanized mulching technology in apple Orchard. Master dissertation. Yangling: Northwest A&F University, 2017; 53p. (in Chinese)

[27] Yang S M, She H Y, Yang S C, Zhu X J, Chen Y, Li J H, et al. Design and experimental validation of improved grapevine burying machine. Int J Agric & Biol Eng, 2018; 11(2): 95–100.

[28] Dai F, Guo W, Song X, Shi R, Zhao W Y, Zhang F W. Design and test of crosswise belt type whole plastic-film ridging-mulching corn seeder on double ridges. Int J Agric & Biol Eng, 2019; 12(4): 88–96.

[29] Xu H Z, Tian D Y, Liu J D, Niu Z H, Li Q. Operation analysis and parameter optimization of drum type soil-covering device. Int J Agric & Biol Eng, 2021; 14(3): 123–129.

[30] Bai G S, Zhou C Y, Du She Ni, Zheng S L, Liu, Y J. Effects of dense planting pattern on the growth of apple tree in Weibei dry plateau. Journal of Zhejiang University, 2019; 45(6): 667–674.

[31] Zhai Z P, Wu Y M, Wang C G. Dynamic simulation and high-speed camera analysis on materials moving along throwing impellers. Transactions of the CSAE, 2012; 28(2): 23–28. (in Chinese)

[32] Zang J J, Zhu X H, Xu S J. Design and test of soil throwing wheel of orchard straw mulching machine. Journal of China Agricultural University, 2020; 25(5): 47–58. (in Chinese)

[33] Hang C G, Gao X J, Yuan M C, Huang Y X, Zhu R X. Discrete element simulations and experiments of soil disturbance as affected by the tine spacing of subsoiler. Biosystems Engineering, 2018; 168: 73–82.

[34] Guo Y. Effect of fly-wheel cutterhead with different curve edges on cutting energy consumption. Journal of Jilin Agricultural University, 2003; 25(1): 107–110. (in Chinese)